AIP | The Journal of Chemical Physics

Assessment of TD-DFT and LF-DFT for study of d − d transitions in first row transition metal hexaaqua complexes

Filip Vlahović, Marko Perić, Maja Gruden-Pavlović, and Matija Zlatar

Citation: The Journal of Chemical Physics **142**, 214111 (2015); doi: 10.1063/1.4922111
View online: http://dx.doi.org/10.1063/1.4922111
View Table of Contents: http://scitation.aip.org/content/aip/journal/jcp/142/21?ver=pdfcov
Published by the AIP Publishing

Assessment of TD-DFT and LF-DFT for study of $d - d$ transitions in first row transition metal hexaaqua complexes

Filip Vlahović,[1] Marko Perić,[2] Maja Gruden-Pavlović,[3] and Matija Zlatar[2,a)]
[1]*Innovation center of the Faculty of Chemistry, University of Belgrade, Studentski trg 12-16, 11000 Belgrade, Republic of Serbia*
[2]*Department of Chemistry, Institute of Chemistry, Technology and Metallurgy, University of Belgrade, Njegoševa 12, 11000 Belgrade, Republic of Serbia*
[3]*Faculty of Chemistry, University of Belgrade, Studentski trg 12-16, 11000 Belgrade, Republic of Serbia*

(Received 12 March 2015; accepted 24 May 2015; published online 5 June 2015)

Herein, we present the systematic, comparative computational study of the $d - d$ transitions in a series of first row transition metal hexaaqua complexes, $[M(H_2O)_6]^{n+}$ ($M^{2+/3+}$ = $V^{2+/3+}$, $Cr^{2+/3+}$, $Mn^{2+/3+}$, $Fe^{2+/3+}$, $Co^{2+/3+}$, Ni^{2+}) by the means of Time-dependent Density Functional Theory (TD-DFT) and Ligand Field Density Functional Theory (LF-DFT). Influence of various exchange-correlation (XC) approximations have been studied, and results have been compared to the experimental transition energies, as well as, to the previous high-level *ab initio* calculations. TD-DFT gives satisfactory results in the cases of d^2, d^4, and low-spin d^6 complexes, but fails in the cases when transitions depend only on the ligand field splitting, and for states with strong character of double excitation. LF-DFT, as a non-empirical approach to the ligand field theory, takes into account in a balanced way both dynamic and non-dynamic correlation effects and hence accurately describes the multiplets of transition metal complexes, even in difficult cases such as sextet-quartet splitting in d^5 complexes. Use of the XC functionals designed for the accurate description of the spin-state splitting, e.g., OPBE, OPBE0, or SSB-D, is found to be crucial for proper prediction of the spin-forbidden excitations by LF-DFT. It is shown that LF-DFT is a valuable alternative to both TD-DFT and *ab initio* methods. © *2015 AIP Publishing LLC*. [http://dx.doi.org/10.1063/1.4922111]

I. INTRODUCTION

Complete understanding of the electronic structure of transition-metal (TM) compounds requires explorations that go beyond solely of a ground states. Consequently, a knowledge of the electronic transitions in TM complexes is essential for understanding their physics and chemistry, for instance, in catalysis, electrochemistry, photochemistry, and biochemistry.[1] In addition to the experiment, computational simulations are very useful tools for understanding and predicting the excitation energies of various systems. In many situations, there may be some experimental uncertainties, and then computational modeling of the excited states becomes essential. For example, when the large number of the excitations is in small energy range, when the excitations are dipole (e.g., in octahedral coordination) or spin-forbidden, when excitations of interest are spectroscopically dark, or with a short lifetime. Adequate treatment of the excited states remains a challenge for theoretical chemistry,[2–4] because it is compulsory to deal with both dynamic and non-dynamic correlation effects equally well. TM compounds are particularly challenging in this respect, because of numerous close lying states stemming from the *d*-orbitals of central metal ion.[4–7]

There is a broad palette of electronic structure methods for excited states,[8] exploited with various success for different problems.[2–4,7] Standard coordination chemistry relies on the Ligand Field Theory (LFT) to interpret and rationalize diverse experimental data of TM systems, e.g., colors, electronic absorption spectra, EPR, and magnetism.[1,9,10] LFT has been recently employed even to interpret complicated high-level *ab initio* results.[11] However, due to its empirical nature, LFT is limited to a description of the data, and predictions are often restricted to a chemical intuition.

High level, wave-function based *ab initio* methods, like complete active space self-consistent field (CASSCF),[12] CAS second-order perturbation theory (CASPT2),[13] *n*-electron valence state perturbation theory (NEVPT2),[14] multi-reference configuration interaction (MRCI),[15] and spectroscopically oriented configuration interaction (SORCI),[16] are, at least in principle, perfectly suitable for modeling of TM complexes and their excited states.[7,17–19] Nevertheless, their success immensely relies upon wise selection of the active space and basis set. Occasionally, large deviations from the experimental transition energies have been reported, e.g., sextet-quartet transitions in $[Fe(H_2O)_6]^{3+}$.[7,20,21] In this case, some authors questioned the experimental interpretation of the spectrum,[20,21] while others claim this system is particularly difficult for *ab initio* calculations.[7] In addition, these approaches, as well as other highly correlated schemes, e.g., equation-of-motion coupled cluster (EOMCC)[22] and algebraic diagrammatic construction (ADC),[23,24] that are rarely used in TM chemistry, are still not suitable for the treatment of large molecules.

Another realm of theoretical chemistry is governed by Density Functional Theory (DFT).[25,26] DFT emerged in the mainstream of computational methods, because of its good

a)Author to whom correspondence should be addressed. Electronic mail: matijaz@chem.bg.ac.rs

compromise between the accuracy and the computational efficiency, and it often provides better results than the other methods, specially when dealing with properties of TM complexes.[6,27–30] Nevertheless, application of DFT in coordination chemistry has shown to be associated with some shortcomings, mainly due to the approximate nature of exchange-correlation (XC) functionals used in practical computations.[6,31–33] Concerning electron excitations, DFT was first used in the framework of ΔSCF approach.[27,28,34–36] The most popular DFT based method for the calculations of excited states is the Time-Dependent Density Functional Theory (TD-DFT),[37–41] despite its well-known drawbacks.[4,40–43] In the area of organic chemistry, TD-DFT is often a method of choice for studying excited states[44,45] and is frequently used in inorganic chemistry.[4,6,46–48] Description of multiplets by TD-DFT is given by linear combination of single excitations. Despite its popularity, some particularly difficult cases for TD-DFT have been reported, e.g., Cr^{3+} complexes[49–51] or $[Ni(H_2O)_6]^{2+}$.[7] Another method which has been proven to perform remarkably well in the determination and understanding of various physical variables, and is also computationally cheap, is Ligand Field Density Functional Theory (LF-DFT).[52,53] This model combines the multideterminantal DFT-based method[34,35,54] and LFT. Readers are referred to the excellent reviews that explain thoroughly the theory behind it.[49,53,55–57] LF-DFT has been used with success to describe ground and excited electronic states originating from d^n TM ions in their complexes,[51–53] for calculation of the hyperfine-coupling parameters,[58] NMR shielding,[59] electronic structure and transitions in f-elements,[60–62] zero-field splitting,[63,64] spin-orbit coupling,[65] and magnetic exchange coupling.[66] Particular flavor of LF-DFT is that it successfully combines the CI and the Kohn-Sham–DFT (KS–DFT) approaches. In doing so, both dynamical correlation (via the DFT XC potential) and non-dynamical correlation (via CI) are considered.

In the present work, we report systematic computational evaluation of the $d-d$ transitions in a series of d^2-d^8 hexaaqua coordinated transition metal ion complexes, $[M(H_2O)_6]^{2+/3+}$, where $M^{2+/3+}$ is $V^{2+/3+}$, $Cr^{2+/3+}$, $Mn^{2+/3+}$, $Fe^{2+/3+}$, $Co^{2+/3+}$, Ni^{2+} (Fig. 1) by TD-DFT and LF-DFT. The primary aim is to investigate the performance of TD-DFT and LF-DFT in predicting the $d-d$ spectra of TM complexes. As both methods, although conceptually different, are based on DFT, the suitability of various XC approximations and their influence on the quality of the results are studied. We will try to address some of the previously mentioned issues concerning electronic excitations in these systems. First, to check if the failure of TD-DFT to reproduce experimental values of Cr^{3+} complexes[49–51] and $[Ni(H_2O)_6]^{2+}$ [7] is inherent to DFT, or it is a consequence of nature of the transitions. Second, whether the experimental assignation of the spectrum of $[Fe(H_2O)_6]^{3+}$ is appropriate.[7,20,21] The series of TM aqua complexes was chosen due to the vast number of experimental[67–83] and computational results[7,20,49,84–90] available for the assessment of the success of both the methods. In addition to the comparison of the results to the spectroscopic studies,[74–83] attention is payed to the comparison of our results to the recent high-level *ab initio* calculations by Neese *et al.*[7] and Schatz *et al.*[20] that were performed on the same series of molecules.

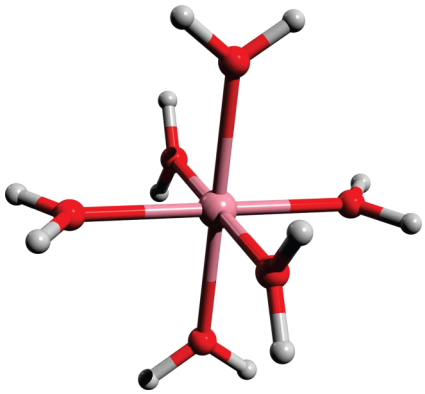

FIG. 1. The structure of investigated hexaaqua transition metal ion complexes, $[M(H_2O)_6]^{n+}$ ($M^{2+/3+} = V^{2+/3+}$, $Cr^{2+/3+}$, $Mn^{2+/3+}$, $Fe^{2+/3+}$, $Co^{2+/3+}$, Ni^{2+}) in T_h symmetry.

II. COMPUTATIONAL DETAILS

The calculations using the unrestricted formalism have been performed with the Amsterdam Density Functional (ADF)[91–93] program package, version 2013.01. All electron Triple-zeta Slater-type orbitals (STO) plus one polarization (TZP) function basis set has been used for all the atoms. All the complexes are treated in the high-spin electron configuration, except $[Co(H_2O)_6]^{3+}$, which is the only one known to have the low-spin ground state.[94] Symmetry constrained geometry optimizations in D_{2h} point group were performed with the local-density approximation (LDA),[95] BP86,[96–98] PW91,[99] OPBE,[100–102] and B3LYP[103] XC functionals. TD-DFT calculations, as implemented in ADF program package,[104,105] were performed with the BP86, PW91, OPBE, SSB-D,[106] B3LYP, CAM-B3LYP,[107] PBE0,[108,109] OPBE0,[102] M06-L,[110,111] and SAOP[112,113] XC functionals, on the BP86 and PW91 optimized geometries. Spin-forbidden transitions were calculated with the spin-flip formalism[114,115] and Tamm-Dancoff approximation.[116] $d-d$ transitions were identified by examination of the corresponding orbitals involved in the excitations.

LF-DFT calculations were carried out on the BP86 and PW91 optimized geometries, using BP86, PW91, OPBE, SSB-D, B3LYP, CAM-B3LYP, PBE0, and OPBE0 XC functionals. LF-DFT[52,53] is based on a multi-determinant description of the multiplet structures[34,35,54] originating from the d^n configuration of the TM ions in the surrounding of coordinating ligands, by combining the CI and the KS-DFT approaches. Theory behind is well documented.[49,53,56] LFDFT, like in fact LFT itself, is rooted in an effective Hamiltonian theory that states that it is possible to define precisely a Hamiltonian for a sub-system such as the levels of a transition metal ion in a TM complex. This condition is possible, because in Werner-type complexes, the metal-ligand bond is mostly ionic. Briefly, LF-DFT procedure consists of the four following steps: (1) an average of configuration (AOC) spin-restricted calculation with n electrons distributed evenly over the five KS molecular orbitals dominated by metal ion d orbitals; (2) spin-unrestricted calculation of the manifold of all Slater determinants (SD) originating from the d^n shell (45, 120, 210, and 252 SD for $d^{2,8}$, $d^{3,7}$, $d^{4,6}$, and d^5 TM ions, respectively) using the KS AOC

orbitals constructed in previous step; (3) energies of these SD and components of the AOC KS eigenvectors that correspond to the metal ion d functions are used to determine the inter-electronic repulsion parameters—Racah's parameters B and C, as well as, the one-electron 5×5 LF matrix. In the final step, (4) these parameters are used to construct full LF Hamiltonian, which is diagonalized, allowing calculation of all the multiplets using the CI of the full LF manifold. All the non-empirically determined parameters for herein studied transition metal hexaaqua complexes can be found in the supplementary material, Tables S23–S33.[117] Matlab scripts for the preparation of input files for SD calculations, extraction of data from ADF calculations, determination of all the parameters, and calculations of the multiplets can be obtained from the authors upon request.

In all the calculations, the solvent effects of water have been implicitly modeled, according to the conductor-like screening model (COSMO),[118–120] as implemented in ADF.[121]

III. RESULTS AND DISCUSSION

The highest possible symmetry, that can be imposed to the hexaaqua complexes, is T_h, Fig. 1, since the inherent symmetry of the water ligands does not allow the complexes to have perfect octahedral symmetry. T_h point group is not implemented in the ADF program package, and therefore, the lower, D_{2h} symmetry was imposed during the DFT geometry optimizations. This is in line with the previous studies,[20,49,84] and is reasonable, since the spatial orientation of water ligands does not influence the calculated $d - d$ transitions, as the orbitals are mainly localized on a metal center[2] (Fig. 2). It should be pointed out that the $d - d$ transition energies in aqua complexes are also not sensitive for the inclusion of the second coordination sphere.[49,87,88]

In the T_h point group, $d_{x^2y^2}$ and d_{z^2} orbitals belong to the E_g irreducible representation (irrep.), while d_{xy}, d_{xz}, d_{yz} orbitals belong to the T_g irrep. In D_{2h} symmetry, $d_{x^2y^2}$ and d_{z^2} orbitals are totally symmetric (A_g irrep.), while d_{xy}, d_{xz}, d_{yz} orbitals belong to the B_{1g}, B_{2g}, and B_{3g} representations, respectively. In the case of d^3, d^5, low-spin d^6, and d^8 electronic configurations, i.e., in complexes with the non-degenerate ground states, Table I, after geometry optimization in D_{2h} symmetry, orbitals corresponding to the B_{1g}, B_{2g}, and B_{3g} set stay degenerate, as well as $d_{x^2y^2}$ and d_{z^2} orbitals belonging to the A_g representation. Therefore, the number of bands corresponds completely to the perfect T_h point group and they are easily assigned according to the Tanabe-Sugano diagrams for octahedral coordination.

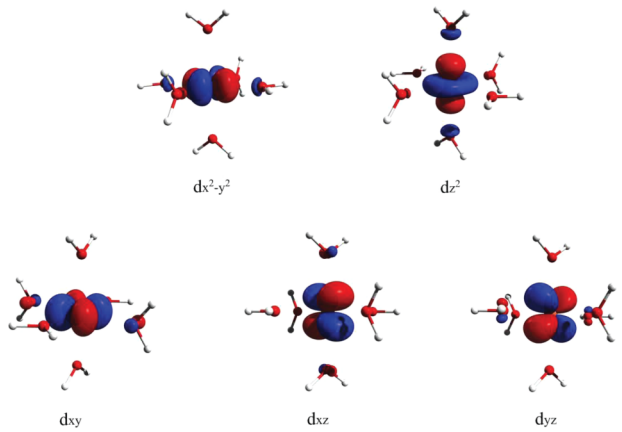

FIG. 2. Molecular orbitals with the dominant metal ion d-character of hexaaqua complexes, obtained from the AOC KS-DFT calculations.

The complexes with the degenerate ground states in T_h point group, i.e., $[V(H_2O)_6]^{3+}$, $[Cr(H_2O)_6]^{2+}$, $[Mn(H_2O)_6]^{3+}$, $[Fe(H_2O)_6]^{2+}$, and $[Co(H_2O)_6]^{2+}$, are prone to the Jahn-Teller (JT) distortion.[122] In the T_h nuclear configuration, they have an E_g or a T_g electronic ground state, depending on the electronic configuration of an investigated molecule, Table I. Such a nuclear configuration is not a stationary point on the potential energy surface, and there is a coupling between the ground electronic state with the non-totally symmetric vibrations, leading to a distorted, D_{2h} structure. Hence, in these cases, orbital degeneracy that would be present in T_h point group is lifted. Consequently, the number of calculated, and experimentally observed, excited states is larger than one would expect simply by taking into account T_h symmetry. It should be noted that, because of single-determinant character of KS reference, TD-DFT in some cases of structures distorted from T_h symmetry is not able to give proper number of excitations.[123] LF-DFT, on the other hand, completely respects the symmetry of the system and predicts correctly all the possible splittings of the electronic states due to the JT distortion. For the sake of simplicity, and easier connection with the experimental explanation of the spectra, assignation of the electronic states for all herein investigated species will be given in T_h symmetry notation.

Optimized M–O bond lengths are listed in Table I. Although, in all cases D_{2h} symmetry was imposed, as aforementioned, complexes with non-degenerate ground state in T_h point group have all bonds and angles equal. For other complexes, as dictated by D_{2h} point group, three pairs of different metal–ligand bond lengths are reported. In general, LDA calculated bond lengths are shorter than experimentally obtained ones. Bond lengths calculated at B3LYP and OPBE levels of theory are slightly longer, but generally in a good agreement with experimental results. On balance, the best agreement with experimental metric data[67–74] was achieved with BP86 and PW91 functionals, and therefore TD-DFT and LF-DFT calculations are employed on the geometries obtained by these two XC functionals. Due to the clarity, and the fact that results do not change significantly depending on the particular geometry used, results on PW91 geometries are collected in the supplementary material, Tables S1–S22.[117]

A. Excitation energies of d^2 complex ion: $[V(H_2O)_6]^{3+}$

Electronic configuration of $[V(H_2O)_6]^{3+}$ complex cation in T_h symmetry is $t_g^2 e_g^0$ leading to the ^3T_g ground state. The lowest excitations belong to the three spin-forbidden triplet to singlet transitions, i.e., $^3T_g \rightarrow {}^1A_g$, $^3T_g \rightarrow {}^1T_g$, and $^3T_g \rightarrow {}^1E_g$, originating from the same $t_g^2 e_g^0$ configuration. The promotion of one electron from the t_g orbitals to the e_g ones results in two ^3T_g ($^3T_{1g}$ and $^3T_{2g}$ in O_h point group), and two ^1T_g excited states ($^1T_{1g}$ and $^1T_{2g}$ in O_h point group). The experimental spectrum of $[V(H_2O)_6]^{3+}$ is characterized

TABLE I. M–O bond distances (Å) for DFT optimized $[M(H_2O)_6]^{2+/3+}$ complex ions ($M^{2+/3+} = V^{2+/3+}$, $Cr^{2+/3+}$, $Mn^{2+/3+}$, $Fe^{2+/3+}$, $Co^{2+/3+}$, Ni^{2+}) with different XC functionals and comparison with available experimental data; where there is more than one distinct M–O bond distance, average (av.) is reported; electronic configuration of a central metal ion and the ground state term in formally T_h point group is indicated.

Complex	Electron configuration	Ground state	LDA	BP86	PW91	OPBE	B3LYP	Expt.	Expt. reference
$[V(H_2O)_6]^{3+}$	d^2	^3T_g	1.915 1.987 1.989 av. 1.964	1.956 2.036 2.039 av. 2.010	1.954 2.034 2.038 av. 2.015	1.956 2.043 2.045 av. 2.015	1.965 2.033 2.039 av. 2.012	1.986 1.987 1.993 av. 1.989	Tregenna-Piggott *et al.*[67]
$[V(H_2O)_6]^{2+}$	d^3	^4A_g	2.058	2.13	2.125	2.147	2.143	2.128	Marcus[68]
$[Cr(H_2O)_6]^{3+}$	d^3	^4A_g	1.926	1.972	1.970	1.974	1.975	1.959	Beattie and Best[69]
$[Cr(H_2O)_6]^{2+}$	d^4	^5E_g	1.998 2.002 2.273 av. 2.091	2.056 2.058 2.391 av. 2.168	2.052 2.059 2.379 av. 2.163	2.061 2.069 2.553 av. 2.228	2.076 2.077 2.368 av. 2.174	2.052 2.122 2.327 av. 2.167	Cotton *et al.*[70]
$[Mn(H_2O)_6]^{3+}$	d^4	^5E_g	1.891 1.895 2.072 av. 1.953	1.934 1.937 2.133 av. 2.001	1.932 1.936 2.130 av. 1.999	1.932 1.939 2.167 av. 2.013	1.936 1.938 2.128 av. 2.001	1.924 1.929 2.129 av. 1.994	Tregenna-Piggott *et al.*[71]
$[Mn(H_2O)_6]^{2+}$	d^5	^6A_g	2.106	2.176	2.174	2.213	2.182	2.192	Marcus[68]
$[Fe(H_2O)_6]^{3+}$	d^5	^6A_g	2.969	2.018	2.016	2.027	2.011	1.995	Beattie and Best[69]
$[Fe(H_2O)_6]^{2+}$	d^6	^5T_g	2.023 2.030 2.112 av. 2.055	2.095 2.100 2.187 av. 2.127	2.086 2.093 2.191 av. 2.123	2.121 2.122 2.244 av. 2.162	2.092 2.112 2.192 av. 2.132	2.098 2.128 2.137 av. 2.121	Becker and Mereiter[72]
$[Co(H_2O)_6]^{3+}$	d^6	^1A_g	1.837	1.885	1.950	1.881	1.885	1.873	Marcus[68]
$[Co(H_2O)_6]^{2+}$	d^7	^4T_g	1.952 2.044 2.046 av. 2.014	2.016 2.113 2.125 av. 2.085	2.016 2.106 2.120 av. 2.081	2.037 2.153 2.160 av. 2.117	2.035 2.108 2.131 av. 2.091	2.044 2.084 2.094 av. 2.074	Stavila *et al.*[73]
$[Ni(H_2O)_6]^{3+}$	d^8	^3A_g	1.979	2.049	2.047	2.074	2.057	2.045	Dobe *et al.*[74]

by two bands, at 17 100 cm^{-1} and at 25 200 cm^{-1},[75] assigned to the two spin-allowed transitions to the ^3T_g excited states.

TD-DFT results are given in Table II, and LF-DFT results in Table III. Splitting of the orbitally triple degenerate ground state in T_h point group due to the JT effect, experimentally observed by the electronic Raman spectra,[76] is reproduced well with both methods. Generally, both TD-DFT and LF-DFT reproduced the experimental spectrum with good accuracy, for the two main transitions, as well as, for the other bands obtained by the Gaussian analysis of the spectrum.[75] It should be noted that TD-DFT calculations at M06-L and SAOP level of theory give very poor results.

Our results are in good agreement with high quality CASSCF/SORCI calculations by Neese *et al.*[7] Recently, Schatz *et al.*[20] calculated the first ^3T_g state with large deviation (CASSCF $\Delta E \sim 5800$ cm^{-1}, CASPT2 $\Delta E \sim 4700$ cm^{-1}, MRCI $\Delta E \sim 5700$ cm^{-1}) from experimental values. CASSCF/CASPT2 calculations by Landry-Hum[85] underestimated the first ^3T_g transition.

B. Excitation energies of d^3 complex ions: $[V(H_2O)_6]^{2+}$ and $[Cr(H_2O)_6]^{3+}$

Ground electronic configuration of $[V(H_2O)_6]^{2+}$ and $[Cr(H_2O)_6]^{3+}$ complexes in T_h symmetry is t_g^3. The ground electronic state in both investigated structures is ^4A_g. The lowest three excitations belong to the spin-flip transitions within the ground t_g^3 electronic configuration, i.e., ^2E_g, ^2T_g, and ^2T_g states. The first two spin-allowed transitions are from the ground ^4A_g state, to the two ^4T_g states, one corresponding to the $^4T_{1g}(F)$ and other to the $^4T_{2g}$ in O_h symmetry. These transitions represent the promotion of the one electron from the t_g orbitals to the e_g orbitals, and transition to the $^4T_{2g}$ state corresponds to the LF splitting Δ. The doublet states originating from the same excited electronic configuration are the two ^2A_g, two ^2E_g, and four ^2T_g. The promotion of the two electrons from the t_g orbitals into the e_g orbitals, without changing the spin gives ^4T_g, $^4T_{1g}(P)$ in O_h notation, as a high lying state. The same excitation, $t_g^3 \rightarrow t_g^1 e_g^2$, accompanied by the spin-flip, gives four ^2T_g states. The excitation of all three

TABLE II. TD-DFT excitation energies (in cm^{-1}) of $[V(H_2O)_6]^{3+}$ with different XC functionals and comparison with available experimental data; mean absolute error (MAE) is given in cm^{-1}; assignment (electronic state and its configuration) in formally T_h point group is indicated.

Assignment	BP86	PW91	OPBE	SSB-D	B3LYP	CAM-B3LYP	PBE0	OPBE0	M06-L	SAOP	Expt.[75]
^3T_g $(t_g^2e_g^0)$	0	0	0	0	0	0	0	0	0	0	0
	2 931	2 859	2 397	3 463	2 676	2 492	2 194	1 290	6 297	12 287	1 940[76]
^1T_g $(t_g^2e_g^0)$	7 127	6 859	9 609	9 294	6 630	6 502	6 900	8 954	13 612	26 625	9 860
	12 687	12 346	15 409	14 908	11 304	11 445	12 602	14 881	18 721	25 629	12 200
^3T_g $(t_g^1e_g^1)$	19 266	19 097	18 046	18 824	18 135	18 032	17 586	16 823	24 019	12 287	17 200
	23 069	22 756	24 161	24 370	22 323	22 381	22 342	23 645	30 390	40 142	19 600
^3T_g $(t_g^1e_g^1)$	24 853	24 679	22 921	24 212	25 658	25 779	25 234	24 121	29 630	28 497	25 200
	26 218	26 576	28 351	28 364	27 234	27 450	27 092	28 437	35 057	44 841	27 900
MAE ($^3\Gamma \rightarrow {}^3\Gamma$)	1 711	1 563	1 719	1 874	1 103	1 039	845	1 217	6 711	11 208	
MAE ($^3\Gamma \rightarrow {}^1\Gamma$)	1 610	1 570	1 730	1 637	2 063	2 056	1 681	1 793	5 136	15 097	
MAE	1 682	1 566	1 722	1 806	1 377	1 329	1 084	1 382	6 261	12 319	

TABLE III. LF-DFT excitation energies (in cm^{-1}) of $[V(H_2O)_6]^{3+}$ with different XC functionals and comparison with available experimental data; mean absolute error (MAE) is given in cm^{-1}; assignment (electronic state and its configuration) in formally T_h point group is indicated.

Assignment	BP86	PW91	OPBE	SSB-D	B3LYP	CAM-B3LYP	PBE0	OPBE0	Expt.[75]
^3T_g $(t_g^2e_g^0)$	0	0	0	0	0	0	0	0	0
	909	899	841	900	855	844	837	798	1 940[76]
	1 092	1 086	1 074	1 056	961	930	955	941	
^1T_g $(t_g^2e_g^0)$	9 654	9 557	10 520	10 407	9 506	9 494	10 006	10 713	9 860
	10 611	10 508	11 479	11 320	10 319	10 300	10 811	11 512	12 200
	11 032	10 925	11 857	11 763	10 772	10 731	11 254	11 931	
^3T_g $(t_g^1e_g^1)$	15 255	15 212	14 814	14 408	14 995	15 229	15 146	14 848	17 200
	16 235	16 186	15 776	15 351	15 829	16 025	15 974	15 663	19 600
	17 590	17 547	17 221	16 697	17 374	17 687	16 697	17 309	
^3T_g $(t_g^1e_g^1)$	23 862	23 796	22 909	22 882	24 047	24 134	23 755	23 193	25 200
	25 884	25 811	24 900	24 917	26 285	26 493	26 016	25 429	27 900
	27 159	27 079	26 150	26 159	27 442	27 621	27 162	26 556	
MAE ($^3\Gamma \rightarrow {}^3\Gamma$)	1 424	1 472	1 986	2 173	1 447	1 290	1 492	1 844	
MAE ($^3\Gamma \rightarrow {}^1\Gamma$)	792	893	596	602	1 004	1 025	656	665	
MAE	1 243	1 306	1 589	1 724	1 320	1 214	1 253	1 507	

electrons from the t_g orbitals to the e_g orbitals, i.e., $^4A_g \rightarrow {}^2E_g$ is also spin forbidden. Only three transitions are observed in the case of $[V(H_2O)_6]^{2+}$, and four transitions in the case of $[Cr(H_2O)_6]^{3+}$ complex cation.[77]

TD-DFT failed to reproduce experimental data for both $[V(H_2O)_6]^{2+}$ and $[Cr(H_2O)_6]^{3+}$, Tables IV and V, in particular relative position of the first two bands. Furthermore, adiabatic TD-DFT is not able to calculate the experimentally observed[77] double excitation ($t_g^3 \rightarrow t_g^1e_g^2$). However, the spin-forbidden transition, $^4A_g \rightarrow {}^2E_g$, of $[Cr(H_2O)_6]^{3+}$ is calculated with very good accuracy with B3LYP, BP86, PW91, and CAM-B3LYP.

In contrast, LF-DFT shows remarkably well performance for both $[V(H_2O)_6]^{2+}$ and $[Cr(H_2O)_6]^{3+}$, Tables VI and VII, and the only discrepancy is observed at CAM-B3LYP level of theory for $[V(H_2O)_6]^{2+}$, because of the overestimation of the ligand-field splitting, Table S23 in the supplementary material.[117] The results are comparable with previous INDO/S,[86] SORCI,[7] and MRCI[20] calculations. In addition, in the case of $[Cr(H_2O)_6]^{3+}$, the third spin-allowed transition, arising from the double excitation, is calculated with even higher precision with LF-DFT than with *ab initio* methods. LF-DFT results are more reliable than recent CASSCF/CASPT2[20] calculations. The transition to the first ^4T_g state, experimentally found at 17 400 cm^{-1}, was calculated with the deviation of ~3800 cm^{-1} (CASSCF) and ~3100 cm^{-1} (CASPT2), while the transition experimentally found at 37 800^{-1} was calculated with the error of ~3300 cm^{-1} using CASPT2.[20]

High overestimation of the first transition to the ^4T_g excited state by TD-DFT is obviously due to the lack of orbital relaxation. Lack of orbital relaxation in TD-DFT has been recently analyzed by Ziegler *et al.*[43] In TM complexes, this is particularly an important issue for the excitations that depend only on the ligand field splitting Δ, like in these two cases ($^4A_{2g}$ to $^4T_{2g}$). On the other hand, orbitals used in LF-DFT are prepared in variational DFT-AOC-SCF procedure, circumventing problems related to the orbital relaxation. Another important issue in d^3 systems is CI mixing between $^4T_{1g}(F)$ and $^4T_{1g}(P)$ states. Because latter one is nominally due to

TABLE IV. TD-DFT excitation energies (in cm^{-1}) of $[V(H_2O)_6]^{2+}$ with different XC functionals and comparison with available experimental data; mean absolute error (MAE) is given in cm^{-1}; assignment (electronic state and its configuration) in formally T_h point group is indicated.

Assignment	BP86	PW91	OPBE	SSB-D	B3LYP	CAM-B3LYP	PBE0	OPBE0	M06-L	SAOP	Expt.[77]
$^4A_g\ (t_g^3e_g^0)$	0	0	0	0	0	0	0	0	0	0	0
$^4T_g\ (t_g^2e_g^1)$	17 435	17 201	15 827	16 813	16 466	16 335	15 702	14 630	23 298	24 474	12 350
$^4T_g\ (t_g^2e_g^1)$	20 010	18 483	18 496	19 460	20 753	20 781	20 407	19 421	26 026	27 121	18 500
$^4T_g\ (t_g^1e_g^2)$	…	…	…	…	…	…	…	…	…	…	27 900
MAE	3 297	2 434	1 740	2 711	3 184	3 133	2 629	1 600	9 237	10 372	

TABLE V. TD-DFT excitation energies (in cm^{-1}) of $[Cr(H_2O)_6]^{3+}$ with different XC functionals and comparison with available experimental data; mean absolute error (MAE) is given in cm^{-1}; assignment (electronic state and its configuration) in formally T_h point group is indicated.

Assignment	BP86	PW91	OPBE	SSB-D	B3LYP	CAM-B3LYP	PBE0	OPBE0	M06-L	SAOP	Expt.[77]
$^4A_g\ (t_g^3e_g^0)$	0	0	0	0	0	0	0	0	0	0	0
$^2E_g\ (t_g^3e_g^0)$	16 295	15 969	19 876	19 414	15 890	16 183	17 614	20 680	24 392	32 569	15 000
$^4T_g\ (t_g^2e_g^1)$	21 410	21 308	19 388	20 748	21 158	21 246	20 451	19 266	26 403	25 872	17 400
$^4T_g\ (t_g^2e_g^1)$	23 512	23 422	21 390	22 792	25 305	25 642	25 057	19 254	28 451	27 617	24 600
$^4T_g\ (t_g^1e_g^2)$	…	…	…	…	…	…	…	…	…	…	37 800
MAE ($^4\Gamma \rightarrow {}^4\Gamma$)	2 549	2 543	2 599	2 578	2 231	2 444	1 754	3 606	6 427	5 744	
MAE ($^4\Gamma \rightarrow {}^2\Gamma$)	1 295	969	4 876	4 414	890	1 183	2 614	5 680	9 329	17 569	
MAE	2 131	2 018	3 358	3 190	1 784	2 023	2 041	4 297	7 415	9 686	

TABLE VI. LF-DFT excitation energies (in cm^{-1}) of $[V(H_2O)_6]^{2+}$ with different XC functionals and comparison with available experimental data; mean absolute error (MAE) is given in cm^{-1}; assignment (electronic state and its configuration) in formally T_h point group is indicated.

Assignment	BP86	PW91	OPBE	SSB-D	B3LYP	CAM-B3LYP	PBE0	OPBE0	Expt.[77]
$^4A_g\ (t_g^3e_g^0)$	0	0	0	0	0	0	0	0	0
$^4T_g\ (t_g^2e_g^1)$	12 311	12 343	11 605	11 563	12 899	15 251	13 048	12 432	12 350
$^4T_g\ (t_g^2e_g^1)$	18 189	18 107	17 119	17 206	18 864	21 228	19 006	18 217	18 500
$^4T_g\ (t_g^1e_g^2)$	28 266	28 148	26 605	26 743	29 332	33 431	29 566	28 322	27 900
MAE	239	216	1 140	1 079	782	3 720	957	262	

TABLE VII. LF-DFT excitation energies (in cm^{-1}) of $[Cr(H_2O)_6]^{3+}$ with different XC functionals and comparison with available experimental data; mean absolute error (MAE) is given in cm^{-1}; assignment (electronic state and its configuration) in formally T_h point group is indicated.

Assignment	BP86	PW91	OPBE	SSB-D	B3LYP	CAM-B3LYP	PBE0	OPBE0	Expt.[77]
$^4A_g\ (t_g^3e_g^0)$	0	0	0	0	0	0	0	0	0
$^2E_g\ (t_g^3e_g^0)$	12 886	12 769	14 325	14 120	12 674	12 758	13 630	14 736	15 000
$^4T_g\ (t_g^2e_g^1)$	17 078	17 043	16 665	16 167	16 730	16 861	16 812	16 559	17 400
$^4T_g\ (t_g^2e_g^1)$	24 052	24 004	23 182	22 950	24 102	24 245	23 998	23 497	24 600
$^4T_g\ (t_g^1e_g^2)$	37 718	37 642	36 518	35 900	37 562	37 801	37 482	36 760	37 800
MAE ($^4\Gamma \rightarrow {}^4\Gamma$)	317	370	1 145	1 594	469	298	503	995	
MAE ($^4\Gamma \rightarrow {}^2\Gamma$)	2 114	2 231	675	880	2 326	2 242	1 370	264	
MAE	766	835	1 027	1 416	933	784	719	812	

TABLE VIII. TD-DFT excitation energies (in cm^{-1}) of $[Cr(H_2O)_6]^{2+}$ with different XC functionals and comparison with available experimental data; mean absolute error (MAE) is given in cm^{-1}; assignment (electronic state and its configuration) in formally T_h point group is indicated.

Assignment	BP86	PW91	OPBE	SSB-D	B3LYP	CAM-B3LYP	PBE0	OPBE0	M06-L	SAOP	Expt.[78]
^5E_g $(t_g^3e_g^1)$	0	0	0	0	0	0	0	0	0	0	0
	8 070	7 800	7 313	8 443	7 973	7 864	7 709	7 246	12 385	14 066	8 000
^5T_g $(t_g^2e_g^2)$	15 277	15 219	14 156	15 102	14 697	14 576	14 288	13 583	20 988	20 536	14 550
	17 424	17 336	16 128	17 196	16 431	16 233	16 023	14 831	23 121	22 464	18 050
	18 006	17 946	16 329	17 574	17 063	16 948	16 089	15 306	23 375	22 506	
MAE	377	426	967	553	492	540	849	1 567	5 340	5 495	

TABLE IX. LF-DFT excitation energies (in cm^{-1}) of $[Cr(H_2O)_6]^{2+}$ with different XC functionals and comparison with available experimental data; mean absolute error (MAE) is given in cm^{-1}; assignment (electronic state and its configuration) in formally T_h point group is indicated.

Assignment	BP86	PW91	OPBE	SSB-D	B3LYP	CAM-B3LYP	PBE0	OPBE0	Expt.[78]
^5E_g $(t_g^3e_g^1)$	0	0	0	0	0	0	0	0	0
	7 308	7 229	6 820	7 019	7 362	7 461	7 304	7 028	8 000
^5T_g $(t_g^2e_g^2)$	13 069	12 988	12 376	12 278	12 824	13 034	12 839	12 428	14 550
	13 075	12 995	12 501	12 407	13 090	13 339	13 070	12 577	18 050
	15 139	15 037	14 325	14 382	14 817	14 984	14 750	14 178	
MAE	1 694	1 780	2 338	2 285	1 821	1 656	1 863	2 297	

TABLE X. TD-DFT excitation energies (in cm^{-1}) of $[Mn(H_2O)_6]^{3+}$ with different XC functionals and comparison with available experimental data; mean absolute error (MAE) is given in cm^{-1}; assignment (electronic state and its configuration) in formally T_h point group is indicated.

Assignment	BP86	PW91	OPBE	SSB-D	B3LYP	CAM-B3LYP	PBE0	OPBE0	M06-L	SAOP	Expt.[79]
^5E_g $(t_g^3e_g^1)$	0	0	0	0	0	0	0	0	0	0	0
	6 554	6 489	5 782	6 827	7 216	7 371	7 104	6 723	9 577	10 048	9 800
^5T_g $(t_g^2e_g^2)$	15 347	15 356	11 636	11 695	18 001	18 550	17 950	16 923	15 858	12 646	20 000
	16 517	16 484	14 313	14 555	19 743	20 651	19 565	18 070	18 641	16 401	21 100
	18 494	18 474	15 701	16 026	20 004	20 876	20 019	18 602	20 037	17 436	
MAE	3 307	3 339	5 481	2 911	1 602	1 017	1 673	2 693	1 345	3 129	

the double excitation from the ground state, this mixing is missing in adiabatic TD-DFT methodology. If we consider LF parameters for $[V(H_2O)_6]^{2+}$ and $[Cr(H_2O)_6]^{3+}$, the double excitation character of, lower, $^4T_{1g}(F)$ state is 16.5% and 9.5%, respectively. This leads to the stabilization of this state due its double excitation character for around 1600 and 1300 cm^{-1}, respectively, which is however in the range of the precision of calculations. LF-DFT, as a non-empirical approach to the LFT, deals very well with such a situation.

C. Excitation energies of d^4 complex ions: $[Cr(H_2O)_6]^{2+}$ and $[Mn(H_2O)_6]^{3+}$

Electronic configuration of $[Cr(H_2O)_6]^{2+}$ and $[Mn(H_2O)_6]^{3+}$ complexes, in T_h symmetry, is $t_g^3e_g^1$, with the ground electronic state ^5E_g. The only spin-allowed excitation belongs to the transition of one electron from the t_g orbitals to the e_g orbitals, resulting in the ^5T_g excited state. Unequal population of the anti-bonding e_g orbitals in the ground state leads to the strong JT distortion that can be clearly reflected in the absorption spectra of these two complexes.[78,79] Instead of the single $^5E_g \rightarrow {}^5T_g$ band, the two major bands are observed—low energy band due to the JT splitting of the ground ^5E_g state, and high energy, broad asymmetric band due to the splitting of the excited ^5T_g state. The spectrum of $[Cr(H_2O)_6]^{2+}$ consists of two major bands centered at 8000 cm^{-1} and 14 550 cm^{-1} with a shoulder at 18 050 cm^{-1} (Tables VIII and IX), and in the spectrum of $[Mn(H_2O)_6]^{3+}$, the bands at around 9800 cm^{-1} and 20 000-21 000 cm^{-1} are observed (Tables X and XI).

TD-DFT reproduced the experimental transitions of $[Cr(H_2O)_6]^{2+}$ with high accuracy, Table VIII, with a mean absolute error (MAE) less than 1000 cm^{-1}. SAOP and M06-L gave transitions intensely shifted toward higher wave-numbers. TD-DFT results for this complex ion are somewhat better than LF-DFT. The first band is well reproduced by LF-DFT regardless of the level of theory, Table IX, while the second transition is underestimated, and shoulder at 18 050 cm^{-1} is not observed, Table IX. Schatz *et al.*[20] highly underestimated the first transition with the error of ~4400 cm^{-1}, 3800 cm^{-1}, and 4700 cm^{-1} with CASSCF, CASPT2, and MRCI, respectively. The second transition was calculated with the deviation of ~3300 cm^{-1} (CASSCF) and ~3100 cm^{-1} (MRCI).[20]

TABLE XI. LF-DFT excitation energies (in cm^{-1}) of $[Mn(H_2O)_6]^{3+}$ with different XC functionals and comparison with available experimental data; mean absolute error (MAE) is given in cm^{-1}; assignment (electronic state and its configuration) in formally T_h point group is indicated.

Assignment	BP86	PW91	OPBE	SSB-D	B3LYP	CAM-B3LYP	PBE0	OPBE0	Expt.[79]
^5E_g $(t_g^3e_g^1)$	0	0	0	0	0	0	0	0	0
	6 437	6 420	6 286	6 474	6 272	6 531	6 475	6 387	9 800
^5T_g $(t_g^2e_g^2)$	16 826	16 800	16 403	16 747	16 041	16 862	16 814	16 619	20 000
	16 984	16 961	16 642	16 809	16 131	16 958	16 861	16 623	21 100
	18 985	18 950	18 498	18 742	18 103	18 839	18 754	18 472	
MAE	2 858	2 883	3 198	2 969	3 479	2 873	2 944	3 140	

Neese *et al.*[89] using CASSCF and SORCI also reported values for the splitting of the ^5E_g term that are underestimated by ~3500–4000 cm^{-1} compared to the experimental observation. The authors suggested that strain influences the splitting of the ^5E_g state, shifting the first experimental transition to the higher energy for approximately 1500 cm^{-1}.[89]

For the case of $[Mn(H_2O)_6]^{3+}$, TD-DFT calculations with B3LYP, M06-L, CAM-B3LYP, and PBE0 show good agreement with the experiment and again show better performance than LF-DFT. Both TD-DFT and LF-DFT match better the experimental spectrum than the recent CASSCF/MRCI study by Schatz *et al.*[20] who obtained the deviation of calculated value for the first transition of ~3400 cm^{-1} (CASSCF) and ~3100 cm^{-1} (MRCI).

LF-DFT calculated ligand-field strength, Δ, Tables S30 and S31 in the supplementary material,[117] for both $[Cr(H_2O)_6]^{2+}$ and $[Mn(H_2O)_6]^{3+}$ in perfect octahedral coordination, is in agreement with the high-level *ab initio* calculations by Neese *et al.*, Figure 3.

D. Excitation energies of d^5 complex ions: $[Mn(H_2O)_6]^{2+}$ and $[Fe(H_2O)_6]^{3+}$

Electronic configuration of $[Mn(H_2O)_6]^{2+}$ and $[Fe(H_2O)_6]^{2+}$ complex in T_h symmetry is $t_g^3e_g^2$, with ground electronic state ^6A_g. There are no spin-allowed $d-d$ transitions in d^5 high spin configuration. The lowest excitations (two ^4A_g, two ^4E_g, two ^4T_g, three ^2A_g, three ^2E_g, four ^1T_g, and four ^1T_g) are the spin-flip transitions originating from the same electronic configuration. Transition of one electron from the t_g orbitals to the e_g orbitals gives the two ^4T_g, two ^2A_g, two ^2E_g, and four ^2T_g excited states. Promotion of the two electrons from the t_g orbitals to the e_g orbitals results in the two ^2T_g states. Experimentally, quartet states are seen in the spectrum, as low-intensity bands, five in the case of $[Mn(H_2O)_6]^{2+}$,[80] and three in the case of $[Fe(H_2O)_6]^{3+}$.[81]

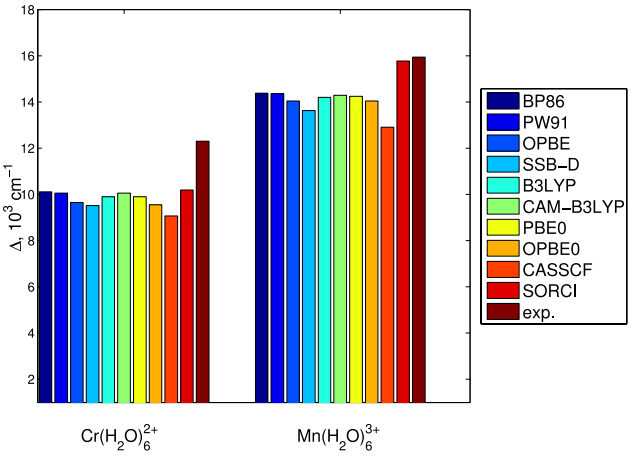

FIG. 3. Ligand field strength of $[Cr(H_2O)_6]^{2+}$ and $[Mn(H_2O)_6]^{3+}$ from LF-DFT calculations with different XC functionals, and comparison with CASSCF and SORCI results of Neese *et al.*[7] and experiment.[78,79]

In $[Mn(H_2O)_6]^{2+}$, the five bands are attributed to the transitions from the ^6A_g ground state to the two ^4T_g ($^4T_{1g}$ and $^4T_{2g}$ in O_h point group), $^4E_g + {}^4A_g$ states, ^4T_g and ^4E_g states, respectively. TD-DFT results, Table XII, are in poor agreement with the experiment. Position of the bands, on the other hand, is excellently reproduced with LF-DFT approach, at SSB-D, PBE0, OPBE0, and OPBE levels of theory, Table XIII.

Spectrum of $[Fe(H_2O)_6]^{3+}$ is characterized by the three absorption bands at 12 600 cm^{-1}, 18 500 cm^{-1}, and 24 300 cm^{-1}.[81] These are the transitions from the ^6A_g ground state to the two ^4T_g ($^4T_{1g}$ and $^4T_{2g}$ in O_h point group), and $^4E_g + {}^4A_g$ states, respectively. TD-DFT calculations failed to reproduce experimental transitions, Table XIV. LF-DFT transitions agree rather well with the experimental values, Table XV. The best agreement was achieved with OPBE0, SSB-D, and OPBE XC functionals.

LF-DFT vertical excitation energies are also in a good agreement with the previously reported INDO/S calculations.[86] Furthermore, LF-DFT is significantly better than the high level wave-function based methods.[7,20,21] In general, wave-function based, post-Hartree-Fock (HF) methods tend to highly overestimate transitions in d^5 TM ion systems. This is because of the importance of the dynamic correlation in the sextet-quartet splitting. Electron correlation between the electrons of opposite spins is completely missing in the HF, and in the post-HF methods, very extensive correlation treatments, with very large basis sets, are needed to achieve more precise results. As already mentioned, these correlation effects are included in LF-DFT through the XC functional. Returning to the question of the reliability of the experimental spectrum of $[Fe(H_2O)_6]^{3+}$,[7,20,21] our LF-DFT results confirm the experimental assignment.

E. Excitation energies of d^6 complex ions: $[Fe(H_2O)_6]^{2+}$ and $[Co(H_2O)_6]^{3+}$

$[Fe(H_2O)_6]^{2+}$ is a high-spin d^6 complex ion, with the $t_g^4e_g^2$ electronic configuration in the T_h point group, and ^5T_g ground electronic state. One spin-allowed transition to the ^5E_g excited

TABLE XII. TD-DFT excitation energies (in cm^{-1}) of $[Mn(H_2O)_6]^{2+}$ with different XC functionals and comparison with available experimental data; mean absolute error (MAE) is given in cm^{-1}; assignment (electronic state and its configuration) in formally T_h point group is indicated.

Assignment	BP86	PW91	OPBE	SSB-D	B3LYP	CAM-B3LYP	PBE0	OPBE0	M06-L	SAOP	Expt.[80]
$^6A_g\ (t_g^3e_g^2)$	0	0	0	0	0	0	0	0	0	0	0
$^4T_g\ (t_g^4e_g^1)$	20 134	19 785	26 952	27 811	18 964	18 978	21 679	27 137	32 131	42 723	18 870
$^4T_g\ (t_g^4e_g^1)$	20 257	19 908	27 063	27 918	19 955	20 038	22 932	28 374	32 253	42 832	23 120
$^4A_g + {}^4E_g\ (t_g^3e_g^2)$	24 720 25 238	24 397 24 890	30 816 31 529	36 308 32 496	23 840 23 885	24 040 24 066	26 400 26 504	31 391 31 471	36 308 37 053	45 574 46 565	24 960 25 270
$^4T_g\ (t_g^3e_g^2)$	25 832	25 445	32 470	32 742	24 382	24 458	27 376	32 747	38 007	47 943	27 980
$^4E_g\ (t_g^3e_g^2)$	25 841	25 457	32 496	32 771	23 886	25 358	28 011	33 158	38 022	46 902	29 750
MAE	1 742	1 983	5 229	6 682	2 537	2 204	1 335	5 721	10 637	20 431	

TABLE XIII. LF-DFT excitation energies (in cm^{-1}) of $[Mn(H_2O)_6]^{2+}$ with different XC functionals and comparison with available experimental data; mean absolute error (MAE) is given in cm^{-1}; assignment (electronic state and its configuration) in formally T_h point group is indicated.

Assignment	BP86	PW91	OPBE	SSB-D	B3LYP	CAM-B3LYP	PBE0	OPBE0	Expt.[80]
$^6A_g\ (t_g^3e_g^2)$	0	0	0	0	0	0	0	0	0
$^4T_g\ (t_g^4e_g^1)$	16 118	15 912	20 105	19 218	15 527	15 606	17 814	20 739	18 870
$^4T_g\ (t_g^4e_g^1)$	20 237	20 038	23 614	22 931	19 695	19 734	21 656	24 146	23 120
$^4A_g + {}^4E_g\ (t_g^3e_g^2)$	22 754	22 547	25 750	25 015	21 834	21 853	23 679	25 922	24 960 25 270
$^4T_g\ (t_g^3e_g^2)$	26 344	26 137	29 264	28 770	25 768	25 768	27 546	29 782	27 980
$^4E_g\ (t_g^3e_g^2)$	28 397	28 188	31 080	30 639	27 760	27 744	29 432	31 498	29 750
MAE	2 197	2 403	996	463	2 850	2 826	942	1 450	

TABLE XIV. TD-DFT excitation energies (in cm^{-1}) of $[Fe(H_2O)_6]^{3+}$ with different XC functionals and comparison with available experimental data; mean absolute error (MAE) is given in cm^{-1}; assignment (electronic state and its configuration) in formally T_h point group is indicated.

Assignment	BP86	PW91	OPBE	SSB-D	B3LYP	CAM-B3LYP	PBE0	OPBE0	M06-L	SAOP	Expt.[81]
$^6A_g\ (t_g^3e_g^2)$	0	0	0	0	0	0	0	0	0	0	0
$^4T_g\ (t_g^4e_g^1)$	11 757	11 515	16 368	18 197	13 200	13 770	15 350	19 476	22 314	24 024	12 600
$^4T_g\ (t_g^4e_g^1)$	11 893	11 650	16 512	18 311	14 437	15 117	16 916	21 021	22 439	24 369	18 500
$^4A_g + {}^4E_g\ (t_g^3e_g^2)$	17 421 19 309	17 239 19 158	19 329 20 499	20 171 21 255	22 194 26 517	23 676 29 047	24 899 29 644	28 015 31 481	23 587 24 495	24 491 24 608	24 300
MAE	4 461	4 678	3 380	3 124	1 572	2 204	2 435	4 106	4 637	5 847	

TABLE XV. LF-DFT excitation energies (in cm^{-1}) of $[Fe(H_2O)_6]^{3+}$ with different XC functionals and comparison with available experimental data; mean absolute error (MAE) is given in cm^{-1}; assignment (electronic state and its configuration) in formally T_h point group is indicated.

Assignment	BP86	PW91	OPBE	SSB-D	B3LYP	CAM-B3LYP	PBE0	OPBE0	Expt.[81]
$^6A_g\ (t_g^3e_g^2)$	0	0	0	0	0	0	0	0	0
$^4T_g\ (t_g^4e_g^1)$	11 102	10 946	14 112	14 240	10 079	9 990	11 683	13 784	12 600
$^4T_g\ (t_g^4e_g^1)$	16 013	15 866	18 523	18 809	15 313	15 243	16 701	18 481	18 500
$^4A_g + {}^4E_g\ (t_g^3e_g^2)$	21 301	21 155	23 463	23 386	20 663	20 694	22 019	23 597	24 300
MAE	2 328	2 477	790	954	3 115	3 157	1 665	635	

TABLE XVI. TD-DFT excitation energies (in cm^{-1}) of $[Fe(H_2O)_6]^{2+}$ with different XC functionals and comparison with available experimental data; mean absolute error (MAE) is given in cm^{-1}; assignment (electronic state and its configuration) in formally T_h point group is indicated.

Assignment	BP86	PW91	OPBE	SSB-D	B3LYP	CAM-B3LYP	PBE0	OPBE0	M06-L	SAOP	Expt.[82]
^5T_g $(t_g^4e_g^2)$	0	0	0	0	0	0	0	0	0	0	0
^5E_g $(t_g^3e_g^3)$	11 887	11 700	11 699	12 499	10 429	10 324	10 741	10 828	16 938	22 954	8 300
	16 846	16 581	15 743	17 298	14 267	14 075	14 266	13 774	24 047	24 970	10 400
MAE	5 016	4 790	4 371	5 548	2 998	2 849	3 153	2 951	11 142	14 612	

TABLE XVII. LF-DFT excitation energies (in cm^{-1}) of $[Fe(H_2O)_6]^{2+}$ with different XC functionals and comparison with available experimental data; mean absolute error (MAE) is given in cm^{-1}; assignment (electronic state and its configuration) in formally T_h point group is indicated.

Assignment	BP86	PW91	OPBE	SSB-D	B3LYP	CAM-B3LYP	PBE0	OPBE0	Expt.[82]
^5T_g $(t_g^4e_g^2)$	0	0	0		0	0	0	0	0
^5E_g $(t_g^3e_g^3)$	8199	8 289	8008	7885	7632	7508	7476	7198	8 300
	9987	10 037	9638	9533	9355	9237	9171	8821	10 400
MAE	257	187	527	641	856	977	1026	1340	

TABLE XVIII. TD-DFT excitation energies (in cm^{-1}) of $[Co(H_2O)_6]^{3+}$ with different XC functionals and comparison with available experimental data; mean absolute error (MAE) is given in cm^{-1}; assignment (electronic state and its configuration) in formally T_h point group is indicated.

Assignment	BP86	PW91	OPBE	SSB-D	B3LYP	CAM-B3LYP	PBE0	OPBE0	M06-L	SAOP	Expt.[83]
^1A_g $(t_g^6e_g^0)$	0	0	0	0	0	0	0	0	0	0	0
^3T_g $(t_g^5e_g^1)$	11 936	11 882	10 066	11 668	11 610	6 458	9 930	8 547	18 329	18 745	8 000
^3T_g $(t_g^5e_g^1)$	12 175	12 115	10 314	11 829	13 367	12 361	12 119	10 766	18 597	19 091	12 500
^1T_g $(t_g^5e_g^1)$	16 608	16 554	14 799	16 402	17 491	17 716	15 976	14 683	22 783	22 742	16 600
^1T_g $(t_g^5e_g^1)$	19 463	19 409	17 659	19 124	23 818	24 510	23 048	21 734	25 267	24 709	24 900
MAE ($^1\Gamma \rightarrow {}^1\Gamma$)	2 130	2 133	2 126	2 169	2 238	840	1 155	1 140	8 213	8 668	
MAE ($^1\Gamma \rightarrow {}^3\Gamma$)	2 722	2 768	4 521	2 987	986	753	1 238	2 541	3 275	3 166	
MAE	2 426	2 451	3 323	2 578	1 612	797	1 197	1 841	5 744	5 917	

state is expected that corresponds to the ligand field splitting Δ. As a consequence of the ground state JT distortion, excited ^5E_g state splits, and two absorption peaks are observed, one at 8300 cm^{-1} and one at 10 400 cm^{-1}. Splitting of the ground ^5T_g state is experimentally not observed, because of the relatively small JT effect associated to the unequal population of the non-bonding t_g orbitals.

TD-DFT calculations with B3LYP, CAM-B3LYP, OPBE0, and PBE0 reproduced the first component of spin-allowed transition with reasonable accuracy (<2500 cm^{-1}), Table XVI. The second transition is calculated on too high energy. This can be explained in the same way as in the case of d^3 systems, due to the lack of orbital excitation in TD-DFT, since upon descent in symmetry ^5E_g state split into two states.

LF-DFT results are in excellent agreement with the experimental data, Table XVII. The transition energies from LF-DFT are in accordance with previous CASSCF/SORCI calculations by Neese *et al.*[7] The recent CASSCF/CASPT2/MRCI study by Schatz *et al.*[20] calculated first transition with the error larger than the 3000 cm^{-1} depending on the chosen method. This shows an obvious advantage of the low cost DFT based methods.

$[Co(H_2O)_6]^{3+}$ is the only low-spin aqua complex ion in the first row TM series,[94] with the closed shell, ^1A_g ground state. Four bands are observed, positioned at 8000 cm^{-1}, 12 500 cm^{-1}, 16 600 cm^{-1}, and 24 900 cm^{-1}.[83] The first two bands are assigned to the spin-forbidden transitions to the ^3T_g states ($^3T_{1g}$ and $^3T_{2g}$ in O_h point group), and the latter two correspond to the spin-allowed transitions to the two ^1T_g states ($^1T_{1g}$ and $^1T_{2g}$ in O_h point group).[83]

Generally speaking, TD-DFT reproduced experimental spectrum with really good accuracy at BP86 optimized geometry with CAM-B3LYP and PBE0 functionals, Table XVIII. LF-DFT calculations at BP86 optimized geometry performed remarkably well with all XC functionals, Table XIX. LF-DFT results obtained on the BP86 geometries are consistent with the previous LF-DFT calculations at PW91 level at LDA geometry done by Atanasov *et al.*,[49] as well as with SORCI[7] and INDO/S calculations.[86] Furthermore, LF-DFT shows better performance than CASSCF,[7,20] CASPT2, and MRCI calculations.[20] In the CASSCF calculations,[20] the first spin-allowed transition was calculated with the error of ~5400 cm^{-1} and the second ^1T_g with the error of ~4300 cm^{-1}. The same transitions were calculated with the error of ~4900 cm^{-1} and ~3500 cm^{-1} using

TABLE XIX. LF-DFT excitation energies (in cm^{-1}) of $[Co(H_2O)_6]^{3+}$ with different XC functionals and comparison with available experimental data; mean absolute error (MAE) is given in cm^{-1}; assignment (electronic state and its configuration) in formally T_h point group is indicated.

Assignment	BP86	PW91	OPBE	SSB-D	B3LYP	CAM-B3LYP	PBE0	OPBE0	Expt.[83]
^1A_g $(t_g^6e_g^0)$	0	0	0	0	0	0	0	0	0
^3T_g $(t_g^5e_g^1)$	9 271	9 329	7 737	7 403	10 186	10 845	10 734	9 539	8 000
^3T_g $(t_g^5e_g^1)$	13 898	13 958	12 008	11 808	15 115	15 917	15 949	14 436	12 500
^1T_g $(t_g^5e_g^1)$	15 329	15 335	14 718	14 310	15 727	16 127	15 986	15 600	16 600
^1T_g $(t_g^5e_g^1)$	24 590	24 598	23 357	23 167	25 518	26 181	26 281	25 352	24 900
MAE ($^1\Gamma \rightarrow {}^1\Gamma$)	790	783	1 712	2 011	746	877	997	726	
MAE ($^1\Gamma \rightarrow {}^3\Gamma$)	1 334	1 393	377	644	2 400	3 131	3 091	1 737	
MAE	1 062	1 088	1 045	1 328	1 573	2 004	2 044	1 232	

TABLE XX. TD-DFT excitation energies (in cm^{-1}) of $[Co(H_2O)_6]^{2+}$ with different XC functionals and comparison with available experimental data; mean absolute error (MAE) is given in cm^{-1}; assignment (electronic state and its configuration) in formally T_h point group is indicated.

Assignment	BP86	PW91	OPBE	SSB-D	B3LYP	CAM-B3LYP	PBE0	OPBE0	M06-L	SAOP	Expt.[77]
^4T_g $(t_g^5e_g^2)$	0	0	0	0	0	0	0	0	0	0	0
^4T_g $(t_g^4e_g^3)$	12 676	12 501	11 876	14 006	10 102	9 927	9 881	9 488	19 406	19 523	8 100
	13 396	13 236	12 624	14 614	11 161	11 003	10 983	10 547	19 762	20 369	
^2E_g $(t_g^6e_g^1)$	6 791	6 362	11 333	12 864	7 168	7 342	9 443	12 658	17 435	15 685	11 300
	11 481	11 041	16 077	17 705	11 616	11 924	13 295	16 556	22 730	20 165	
^4A_g $(t_g^3e_g^4)$	…	…	…	…	…	…	…	…	…	…	16 000
^4T_g $(t_g^4e_g^3)$	20 146	19 902	18 669	21 799	19 021	18 899	19 240	18 550	29 558	25 253	19 400
	20 748	20 512	19 231	22 257	20 104	20 026	20 309	19 525	30 040	26 016	21 550
MAE ($^4\Gamma \rightarrow {}^4\Gamma$)	2 161	2 103	2 400	3 105	1 452	1 463	1 244	1 597	10 044	7 388	
MAE ($^4\Gamma \rightarrow {}^2\Gamma$)	2 164	2 598	2 405	3 984	1 908	1 667	69	3 307	8 782	6 625	
MAE	2 162	2 227	2 401	3 325	1 566	1 514	950	2 025	9 729	7 197	

the CASPT2 calculations.[20] MRCI gave errors of ~6100 cm^{-1} for the first singlet transition and ~3900 cm^{-1} for the second singlet transition.[20] CASSCF calculations by Neese *et al.*[7] also underestimated the first ^1T_g transition, with the error of ~3900 cm^{-1}.

In the case of PW91 geometry, both LF-DFT and TD-DFT generally failed to reproduce experimental values, Tables S17 and S18 in the supplementary material.[117] This discrepancy is because of too long $Co^{-}O$ bond lengths from the PW91 geometry optimization ($Co^{-}O$ bond lengths: PW91 1.950 Å, BP86 1.885 Å, experimental 1.873 Å, Table I).

F. Excitation energies of d^7 complex ion: $[Co(H_2O)_6]^{2+}$

Electronic configuration of $[Co(H_2O)_6]^{2+}$ complex in T_h symmetry is $t_g^5e_g^2$. The ground electronic state is ^4T_g. Two spin-allowed transitions belong to the promotion of one electron from the t_g orbitals to the e_g orbitals, resulting in the two ^4T_g states ($^4T_{1g}$ and $^4T_{2g}$ in O_h symmetry). Splitting of the second ^4T_g state because of the ground state JT effect is experimentally not observed.[77] Possible spin-forbidden transitions are to the two ^2A_g, two ^2E_g, and four ^2T_g excited states. Promotion of the two electrons from the t_g orbitals to the e_g orbitals gives the one ^4A_g state, one ^2E_g, and two ^2T_g states.

TD-DFT calculations, Table XX, overestimated the first transition to the ^4T_g state, while not able to calculate the two-electron excitation to the ^4A_g state. The third transition is satisfactorily reproduced. It should be noted that M06-L and SAOP completely failed to reproduce the experimental values.

LF-DFT calculations for all three spin-allowed transitions, Table XXI, are in excellent agreement with experiment, regardless of the choice of the XC functional. LF-DFT underestimates the spin-forbidden transition $^4T_g \rightarrow {}^2E_g$, even though results with OPBE, OPBE0, and SSB-D are in the reasonable agreement with the experiment. Our LF-DFT results are in agreement with the previously reported LF-DFT calculations with PW91 functional by Atanasov *et al.*[49]

G. Excitation energies of d^8 complex ion: $[Ni(H_2O)_6]^{2+}$

The ground electronic state of $[Ni(H_2O)_6]^{2+}$ complex in the T_h symmetry is ^3A_g, with the electronic configuration $t_g^6e_g^2$. Three spin-allowed transitions to the ^3T_g excited states ($^3T_{2g}$ corresponding to Δ, and $^3T_{1g}(F)$ and $^3T_{1g}(P)$ states in O_h point group) are observed.[74] The first two transitions originate from the excitation of the one electron from the t_g to the e_g orbital. The third transition is the double excitation from the t_g orbitals

TABLE XXI. LF-DFT excitation energies (in cm^{-1}) of $[Co(H_2O)_6]^{2+}$ geometries with different XC functionals and comparison with available experimental data; mean absolute error (MAE) is given in cm^{-1}; assignment (electronic state and its configuration) in formally T_h point group is indicated.

Assignment	BP86	PW91	OPBE	SSB-D	B3LYP	CAM-B3LYP	PBE0	OPBE0	Expt.[77]
^4T_g $(t_g^5e_g^2)$	0	0	0	0	0	0	0	0	0
^4T_g $(t_g^4e_g^3)$	7 684	7 670	7 363	7 191	7 029	6 890	6 862	6 649	8 100
	8 196	8 185	7 853	7 678	7 300	7 100	7 074	6 832	
	9 368	9 353	9 039	8 813	8 535	8 377	8 342	8 116	
^2E_g $(t_g^6e_g^1)$	5 446	5 336	7 728	7 753	5 580	5 738	6 937	8 546	11 300
	7 540	7 426	9 770	9 785	7 595	7 749	8 904	10 468	
^4A_g $(t_g^3e_g^4)$	17 642	17 616	16 947	16 566	16 121	15 806	15 742	15 274	16 000
^4T_g $(t_g^4e_g^3)$	19 028	19 018	18 005	18 490	18 821	18 618	18 382	17 743	19 400
	20 482	20 468	19 480	19 991	20 299	20 110	19 857	19 225	21 550
	21 453	21 434	20 406	20 892	21 043	20 798	20 534	19 860	
MAE ($^4\Gamma \rightarrow {}^4\Gamma$)	602	594	691	397	317	406	557	1 058	
MAE ($^4\Gamma \rightarrow {}^2\Gamma$)	4 807	4 919	2 551	2 531	4 712	4 556	3 379	1 793	
MAE	1 443	1 459	1 063	824	1 196	1 236	1 122	1 205	

TABLE XXII. TD-DFT excitation energies (in cm^{-1}) of $[Ni(H_2O)_6]^{2+}$ with different XC functionals and comparison with available experimental data; mean absolute error (MAE) is given in cm^{-1}; assignment (electronic state and its configuration) in formally T_h point group is indicated.

Assignment	BP86	PW91	OPBE	SSB-D	B3LYP	CAM-B3LYP	PBE0	OPBE0	M06-L	SAOP	Expt.[74]
^3A_g $(t_g^6e_g^2)$	0	0	0	0	0	0	0	0	0	0	0
^3T_g $(t_g^5e_g^3)$	16 137	15 984	14 355	16 895	14 401	13 926	18 485	14 361	12 814	24 973	8 700
^3T_g $(t_g^5e_g^3)$	19 539	19 388	17 865	20 417	20 417	20 480	20 554	19 544	28 573	21 367	13 750
^1E_g $(t_g^6e_g^2)$	14 105	13 839	15 012	18 134	14 768	15 226	16 269	15 506	24 923	17 344	15 250
^1T_g $(t_g^5e_g^3)$	20 220	19 988	20 711	23 315	20 125	20 244	20 080	21 010	31 693	23 540	22 000
^3T_g $(t_g^4e_g^4)$	…	…	…	…	…	…	…	…	…	…	25 144
MAE ($^3\Gamma \rightarrow {}^3\Gamma$)	6 613	6 461	4 885	7 431	6 184	5 978	8 294	5 727	9 468	11 945	
MAE ($^3\Gamma \rightarrow {}^1\Gamma$)	1 462	1 712	763	2 099	1 178	890	1 469	623	9 683	1 817	
MAE	4 038	4 086	2 824	4 765	3 681	3 434	4 882	3 175	9 576	6 881	

TABLE XXIII. LF-DFT excitation energies (in cm^{-1}) of $[Ni(H_2O)_6]^{2+}$ with different XC functionals and comparison with available experimental data; mean absolute error (MAE) is given in cm^{-1}; assignment (electronic state and its configuration) in formally T_h point group is indicated.

Assignment	BP86	PW91	OPBE	SSB-D	B3LYP	CAM-B3LYP	PBE0	OPBE0	Expt.[74]
^3A_g $(t_g^6e_g^2)$	0	0	0	0	0	0	0	0	0
^3T_g $(t_g^5e_g^3)$	9 529	9 521	9 201	8 992	9 316	9 233	9 229	9 114	8 700
^3T_g $(t_g^5e_g^3)$	15 518	15 506	14 919	14 735	15 273	15 148	15 110	14 870	13 750
^1E_g $(t_g^6e_g^2)$	12 478	12 410	13 258	13 465	12 232	12 218	12 759	13 321	15 250
^1T_g $(t_g^5e_g^3)$	21 647	21 569	22 129	22 089	21 162	21 065	21 614	22 081	22 000
^3T_g $(t_g^4e_g^4)$	26 040	26 026	24 807	25 100	26 059	25 889	25 684	25 061	25 144
MAE ($^3\Gamma \rightarrow {}^3\Gamma$)	1 164	1 153	669	440	1 018	892	810	539	
MAE ($^3\Gamma \rightarrow {}^1\Gamma$)	1 562	1 635	1 060	937	1 928	1 984	1 438	1 005	
MAE	1 324	1 346	825	639	1 382	1 329	1 061	725	

to the e_g ones. Additionally, the two spin-forbidden transitions are experimentally observed.[74]

Our TD-DFT calculations failed to reproduce correctly experimental spectrum, Table XXII, in line with the conclusions of Neese *et al.*[7] Reason behind the failure of TD-DFT to describe the spectrum of $[Ni(H_2O)_6]^{2+}$ is a consequence of two factors. First one is lack of orbital relaxation in TD-DFT,[43] resulting in the overestimation of the first transition that corresponds to the ligand field splitting. The second reason is CI mixing between two $^3T_{1g}$ states. As already mentioned, the

second $^3T_{1g}$ transition corresponds to a double excitation from the ground state and is ignored with adiabatic TD-DFT. Ligand field analysis[124] shows that this mixing is much more significant for $[Ni(H_2O)_6]^{2+}$ than for $[Cr(H_2O)_6]^{3+}$ and $[V(H_2O)_6]^{2+}$. Contribution of the double excitation to the $^3T_{1g}(F)$ is very large, 45%. Thus, this $^3T_{1g}(F)$-$^3T_{1g}(P)$ mixing should lead to the stabilization of $^3T_{1g}(F)$ for around 4600 cm^{-1}. Neese[31] pointed out that TD-DFT predicts only one $^3T_{1g}$ transition, almost half in between experimentally observed $^3T_{1g}(F)$ and $^3T_{1g}(P)$ states.

Consequently, LF-DFT, taking into account all these effects, gives perfect match with the experimental values, Table XXIII, specially with OPBE, OPBE0, and SSB-D functionals. Good agreement with previous INDO/S[86] and with SORCI calculations[7] was achieved, as well.

IV. CONCLUSIONS

In this work, $d-d$ transitions in the series of first row TM aqua complexes have been studied by the means of two DFT based methods. It has been shown that TD-DFT, although being one of the most popular methods for studying excited states, should be used with caution when dealing with $d-d$ excitations of TM complexes. TD-DFT suffers from the large dependence on the chosen XC functional. In general, TD-DFT provides satisfactory results only in the cases of d^2, d^4, and low-spin d^6 TM ion complexes. It should be emphasized that in the case of $[Ni(H_2O)_6]^{2+}$, $[V(H_2O)_6]^{2+}$, and $[Cr(H_2O)_6]^{3+}$, TD-DFT clearly failed because of the lack of orbital relaxation. In the mentioned cases, overestimated first transition depends only on the ligand field splitting Δ. Furthermore, in these systems, second state has substantial character of double excitation, that cannot be accessed by adiabatic TD-DFT. The stronger mixing is, the less accurate results are obtained.

On the other hand, LF-DFT is shown to be accurate for the description of the multiplets in the entire, herein studied series of complex ions. The key feature of this approach is the explicit treatment of the near degeneracy effects using CI within the active space of KS orbitals with dominant TM ion d-electron character. For spin-allowed transitions, LF-DFT does not show substantial dependence on the chosen XC approximation. In the case of spin-forbidden excitations, excellent results were obtained when using XC functionals designed for the accurate description of the spin-state splitting, e.g., with OPBE, OPBE0, or SSB-D. The quality of the LF-DFT is comparable to the high-level *ab initio* calculations,[7,20] and in the case of sextet-quartet transitions in $[Mn(H_2O)_6]^{2+}$ and $[Fe(H_2O)_6]^{3+}$ even outshines them. The reason behind this is that, with a properly chosen XC functional, LF-DFT coherently takes into account both dynamic and non-dynamic correlation effects. Sextet-quartet transitions in Mn^{2+} and Fe^{3+} complexes seem to be a perfect test case for applicability of different XC approximations in LF-DFT, and in fact for other methods that deal with excited states.

In conclusion, herein presented results show that LF-DFT can be considered as a reliable method for studying $d-d$ transitions in TM complexes. It can be regarded as a valuable alternative to both TD-DFT and *ab initio* methods in theoretical inorganic chemistry. LF-DFT takes advantages of both standard ligand field theory and modern DFT and sheds the light on the coordination chemistry of the TM ions. However, since LF-DFT is rooted in LF theory itself, it is not possible to elucidate charge transfer (CT) transitions with this approach. In addition to metal centered, CT transitions are obviously also important and can dominate in the absorption spectra of TM compounds. Combination of multiplet-sum ΔSCF-DFT[35,36] with LF-DFT could be a possible route for the treatment of both CT and $d-d$ transitions. This is currently under development in our group.

ACKNOWLEDGMENTS

This work was supported by the Ministry of Education, Science and Technological Development of the Republic of Serbia under Project No. 172035.

[1]F. A. Cotton, G. Wilkinson, C. A. Murillio, and M. Bochmann, *Advanced Inorganic Chemistry*, 6th ed. (Wiley, Chichester, 1999).
[2]C. Daniel, Coord. Chem. Rev. **238–239**, 143 (2003).
[3]C. Daniel, Coord. Chem. Rev. **282–283**, 19 (2015).
[4]L. Gonzalez, D. Escudero, and L. Serrano-Andres, ChemPhysChem **13**, 28 (2012).
[5]A. Bencini, Inorg. Chim. Acta **361**, 3820 (2008).
[6]C. J. Cramer and D. G. Truhlar, Phys. Chem. Chem. Phys. **11**, 10757 (2009).
[7]F. Neese, T. Petrenko, D. Ganyushin, and G. Olbrich, Coord. Chem. Rev. **251**, 288 (2007).
[8]C. J. Cramer, *Essentials of Computational Chemistry: Theories and Models*, 2nd ed. (Wiley, Chichester, 2004).
[9]E. I. Solomon and A. B. P. Lever, *Inorganic Electronic Structure and Spectroscopy* (John Wiley & Sons, 2006), Chap. 658.
[10]F. Neese, in *Practical Approaches to Biological Inorganic Chemistry*, edited by R. R. Crichton and R. O. Louro (Elsevier, Oxford, 2013), pp. 23–51.
[11]M. Atanasov, D. Ganyushin, K. Sivalingam, and F. Neese, in *Molecular Electronic Structures of Transition Metal Complexes II*, Structure and Bonding Vol. 143, edited by D. M. P. Mingos, P. Day, and J. P. Dahl, (Springer, Berlin, Heidelberg, 2012), pp. 149–220.
[12]D. Hegarty and M. A. Robb, Mol. Phys. **38**, 1795 (1979).
[13]K. Andersson, P. Malmqvist, and B. O. Roos, J. Chem. Phys. **96**, 1218 (1992).
[14]C. Angeli, R. Cimiraglia, S. Evangelisti, T. Leininger, and J.-P. Malrieu, J. Chem. Phys. **114**, 10252 (2001).
[15]R. Buenker and S. Peyerimhoff, Theor. Chim. Acta **12**, 183 (1968).
[16]F. Neese, J. Chem. Phys. **119**, 9428 (2003).
[17]K. Pierloot, Mol. Phys. **101**, 2083 (2003).
[18]S. Vancoillie, H. Zhao, V. T. Tran, M. F. A. Hendrickx, and K. Pierloot, J. Chem. Theory Comput. **7**, 3961 (2011).
[19]M. Atanasov, D. Aravena, E. Suturina, E. Bill, D. Maganas, and F. Neese, Coord. Chem. Rev. **289-290**, 177 (2014).
[20]Y. Yang, M. A. Ratner, and G. C. Schatz, J. Phys. Chem. C **118**, 29196 (2014).
[21]A. Ghosh and P. R. Taylor, Curr. Opin. Chem. Biol. **7**, 113 (2003).
[22]J. F. Stanton and R. J. Bartlett, J. Chem. Phys. **98**, 7029 (1993).
[23]J. Schirmer and A. B. Trofimov, J. Chem. Phys. **120**, 11449 (2004).
[24]A. Dreuw and M. Wormit, WIRES Comput. Mol. Sci. **5**, 82 (2015).
[25]R. G. Parr and W. Yang, *Density-Functional Theory of Atoms and Molecules* (Oxford University Press, 1989).
[26]W. Koch and M. C. Holthausen, *A Chemist's Guide to Density Functional Theory* (Wiley-VCH Verlag GmbH, Weinheim, 2001).
[27]T. Ziegler, Chem. Rev. **91**, 651 (1991).
[28]H. Chermette, Coord. Chem. Rev. **178–180**, 699 (1998).
[29]I. Ciofini and C. A. Daul, Coord. Chem. Rev. **238–239**, 187 (2003).
[30]A. C. Tsipis, Coord. Chem. Rev. **272**, 1 (2014).
[31]F. Neese, J. Biol. Inorg. Chem. **11**, 702 (2006).
[32]M. Swart, Int. J. Quantum Chem. **113**, 2 (2013).
[33]J. N. Harvey, Annu. Rep. Prog. Chem., Sect. C: Phys. Chem. **102**, 203 (2006).
[34]T. Ziegler and A. Rauk, Theor. Chim. Acta **46**, 1 (1977).
[35]C. Daul, Int. J. Quantum Chem. **52**, 867 (1994).
[36]C. Daul, E. J. Baerends, and P. Vernooijs, Inorg. Chem. **33**, 3538 (1994).
[37]E. Runge and E. K. U. Gross, Phys. Rev. Lett. **52**, 997 (1984).

[38]E. K. U. Gross, J. F. Dobson, and M. Petersilka, in *Density Functional Theory II*, Topics in Current Chemistry Vol. 181, edited by R. F. Nalewajski, (Springer-Verlag, Berlin/Heidelberg, 1996), pp. 81–172.
[39]M. E. Casida, in *Recent Developments and Applications of Modern Density Functional Theory*, Theoretical and Computational Chemistry Vol. 4, edited by J. Seminario (Elsevier, 1996), pp. 391–439.
[40]M. E. Casida, J. Mol. Struct.: THEOCHEM **914**, 3 (2009).
[41]M. Casida and M. Huix-Rotllant, Annu. Rev. Phys. Chem. **63**, 287 (2012).
[42]A. Dreuw and M. Head-Gordon, J. Am. Chem. Soc **126**, 4007 (2004).
[43]H. R. Zhekova, M. Seth, and T. Ziegler, Int. J. Quantum Chem. **114**, 1019 (2014).
[44]A. D. Laurent and D. Jacquemin, Int. J. Quantum Chem. **113**, 2019 (2013).
[45]A. D. Laurent, C. Adamo, and D. Jacquemin, Phys. Chem. Chem. Phys. **16**, 14334 (2014).
[46]A. Rosa, G. Ricciardi, O. Gritsenko, and E. Baerends, *Principles and Applications of Density Functional Theory in Inorganic Chemistry I*, Structure and Bonding Vol. 112 (Springer, Berlin, Heidelberg, 2004), pp. 49–116.
[47]T. Le Bahers, E. Bremond, I. Ciofini, and C. Adamo, Phys. Chem. Chem. Phys. **16**, 14435 (2014).
[48]K. Mori, T. P. M. Goumans, E. van Lenthe, and F. Wang, Phys. Chem. Chem. Phys. **16**, 14523 (2014).
[49]M. Atanasov, P. Comba, C. Daul, and F. Neese, in *Models, Mysteries and Magic of Molecules*, edited by J. Boeyens and J. Ogilvie (Springer, Netherlands, 2008), pp. 411–445.
[50]Z. D. Matović, M. S. Jeremić, R. M. Jelić, M. Zlatar, and I. Z. Jakovljević, Polyhedron **55**, 131 (2013).
[51]M. Zlatar, M. Gruden-Pavlović, M. Güell, and M. Swart, Phys. Chem. Chem. Phys. **15**, 6631 (2013).
[52]M. Atanasov, C. Daul, and C. Rauzy, in *Optical Spectra and Chemical Bonding in Inorganic Compounds*, Structure and Bonding edited by D. Mingos and T. Schönherr, (Springer, Berlin, Heidelberg, 2004), Vol. 106, pp. 97–125.
[53]M. Atanasov, C. A. Daul, and C. Rauzy, Chem. Phys. Lett. **367**, 737 (2003).
[54]T. Mineva, A. Goursot, and C. Daul, Chem. Phys. Lett. **350**, 147 (2001).
[55]M. Atanasov and C. Daul, Chimia **59**, 504 (2005).
[56]M. Atanasov and C. Daul, C. R. Chim. **8**, 1421 (2005).
[57]C. Daul, J. Phys.: Conf. Ser. **428**, 012023 (2013).
[58]M. Atanasov, E. Jan Baerends, P. Baettig, R. Bruyndonckx, C. Daul, C. Rauzy, and M. Zbiri, Chem. Phys. Lett. **399**, 433 (2004).
[59]F. Senn, M. Zlatar, M. Gruden-Pavlović, and C. Daul, Monatsh. Chem. **142**, 593 (2011).
[60]M. Atanasov, C. Daul, H. U. Güdel, T. A. Wesolowski, and M. Zbiri, Inorg. Chem. **44**, 2954 (2005).
[61]H. Ramanantoanina, W. Urland, F. Cimpoesu, and C. Daul, Phys. Chem. Chem. Phys. **15**, 13902 (2013).
[62]H. Ramanantoanina, W. Urland, A. Garcia-Fuente, F. Cimpoesu, and C. Daul, Phys. Chem. Chem. Phys. **16**, 14625 (2014).
[63]M. Atanasov, P. Comba, and C. A. Daul, Inorg. Chem. **47**, 2449 (2008).
[64]M. Gruden-Pavlović, M. Perić, M. Zlatar, and P. Garcia-Fernandez, Chem. Sci. **5**, 1453 (2014).
[65]M. Atanasov, C. Rauzy, P. Baettig, and C. Daul, Int. J. Quantum Chem. **102**, 119 (2005).
[66]M. Atanasov and C. A. Daul, Chem. Phys. Lett. **381**, 584 (2003).
[67]P. L. W. Tregenna-Piggott, D. Spichiger, G. Carver, B. Frey, R. Meier, H. g. Weihe, J. A. Cowan, G. J. McIntyre, G. Zahn, and A.-L. Barra, Inorg. Chem. **43**, 8049 (2004).
[68]Y. Marcus, Chem. Rev. **88**, 1475 (1988).
[69]J. K. Beattie and S. P. Best, Coord. Chem. Rev. **166**, 391 (1997).
[70]F. A. Cotton, L. M. Daniels, C. A. Murillo, and J. F. Quesada, Inorg. Chem. **32**, 4861 (1993).
[71]P. L. W. Tregenna-Piggott, H.-P. Andres, G. J. McIntyre, S. P. Best, C. C. Wilson, and J. A. Cowan, Inorg. Chem. **42**, 1350 (2003).
[72]E. Becker, K. Kirchner, and K. Mereiter, Acta Crystallogr., Sect. E: Struct. Rep. Online **65**, i71 (2009).
[73]V. Stavila, I. Bulimestru, A. Gulea, A. C. Colson, and K. H. Whitmire, Acta Crystallogr., Sect. C: Cryst. Struct. Commun. **67**, m65 (2011).
[74]C. Dobe, E. Gonzalez, P. L. W. Tregenna-Piggott, and C. Reber, Dalton Trans. **43**, 17864 (2014).
[75]D. A. Johnson and P. G. Nelson, Inorg. Chem. **38**, 4949 (1999).
[76]S. P. Best and R. J. H. Clark, Chem. Phys. Lett. **122**, 401 (1985).
[77]C. K. Joergensen, "Spectroscopy of transition-group complexes," in *Advances in Chemical Physics* (John Wiley & Sons, Inc., 1963), pp. 33–146.
[78]C. Dobe, C. Noble, G. Carver, P. L. Tregenna-Piggott, G. J. McIntyre, A. L. Barra, A. Neels, S. Janssen, and F. Juranyi, J. Am. Chem. Soc. **126**, 16639 (2004).
[79]P. L. W. Tregenna-Piggott, H. Weihe, and A.-L. Barra, Inorg. Chem. **42**, 8504 (2003).
[80]L. J. Heidt, G. F. Koster, and A. M. Johnson, J. Am. Chem. Soc. **80**, 6471 (1958).
[81]C. K. Joergensen, *Absorption Spectra and Chemical Bonding in Complexes* (Pergamon Press, Oxford, England, United Kingdom, 1962).
[82]F. A. Cotton and M. D. Meyers, J. Am. Chem. Soc. **82**, 5023 (1960).
[83]D. A. Johnson and A. G. Sharpe, J. Chem. Soc. A **1966**, 798.
[84]R. J. Deeth and K. Randell, Inorg. Chem. **47**, 7377 (2008).
[85]J. Landry-Hum, G. Bussière, C. Daniel, and C. Reber, Inorg. Chem. **40**, 2595 (2001).
[86]W. P. Anderson, W. D. Edwards, and M. C. Zerner, Inorg. Chem. **25**, 2728 (1986).
[87]C. M. Aguilar, W. B. D. Almeida, and W. R. Rocha, Chem. Phys. Lett. **449**, 144 (2007).
[88]C. M. Aguilar, W. B. D. Almeida, and W. R. Rocha, Chem. Phys. **353**, 66 (2008).
[89]D. G. Liakos, D. Ganyushin, and F. Neese, Inorg. Chem. **48**, 10572 (2009).
[90]B. Kallies and R. Meier, Inorg. Chem. **40**, 3101 (2001).
[91]C. Fonseca Guerra, J. G. Snijders, G. te Velde, and E. J. Baerends, Theor. Chem. Acc. **99**, 391 (1998).
[92]G. te Velde, F. M. Bickelhaupt, E. J. Baerends, C. Fonseca Guerra, S. J. A. van Gisbergen, J. G. Snijders, and T. Ziegler, J. Comput. Chem. **22**, 931 (2001).
[93]"ADF: Density Functional Theory (DFT) software for chemists, version 2013.01," see http://www.scm.com/, 2013.
[94]R. Aakesson, L. G. M. Pettersson, M. Sandstroem, and U. Wahlgren, J. Am. Chem. Soc **116**, 8691 (1994).
[95]S. H. Vosko, L. Wilk, and M. Nusair, Can. J. Phys. **58**, 1200 (1980).
[96]A. D. Becke, Phys. Rev. A **38**, 3098 (1988).
[97]J. P. Perdew, Phys. Rev. B **33**, 8822 (1986).
[98]J. P. Perdew, Phys. Rev. B **34**, 7406 (1986).
[99]J. P. Perdew, J. A. Chevary, S. H. Vosko, K. A. Jackson, M. R. Pederson, D. J. Singh, and C. Fiolhais, Phys. Rev. B **46**, 6671 (1992).
[100]N. C. Handy and A. J. Cohen, Mol. Phys. **99**, 403 (2001).
[101]J. P. Perdew, K. Burke, and M. Ernzerhof, Phys. Rev. Lett. **77**, 3865 (1996).
[102]M. Swart, A. W. Ehlers, and K. Lammertsma, Mol. Phys. **102**, 2467 (2004).
[103]P. J. Stephens, F. J. Devlin, C. F. Chabalowski, and M. J. Frisch, J. Phys. Chem. **98**, 11623 (1994).
[104]F. Kootstra, P. L. de Boeij, and J. G. Snijders, J. Chem. Phys. **112**, 6517 (2000).
[105]P. Romaniello and P. L. de Boeij, Phys. Rev. B **71**, 155108 (2005).
[106]M. Swart, M. Sola, and F. M. Bickelhaupt, J. Chem. Phys. **131**, 094103 (2009).
[107]T. Yanai, D. P. Tew, and N. C. Handy, Chem. Phys. Lett. **393**, 51 (2004).
[108]M. Ernzerhof and G. E. Scuseria, J. Chem. Phys. **110**, 5029 (1999).
[109]C. Adamo and V. Barone, J. Chem. Phys. **110**, 6158 (1999).
[110]Y. Zhao and D. Truhlar, Theor. Chem. Acc. **120**, 215 (2008).
[111]Y. Zhao and D. G. Truhlar, J. Chem. Phys. **125**, 194101 (2006).
[112]O. Gritsenko, P. Schipper, and E. Baerends, Chem. Phys. Lett. **302**, 199 (1999).
[113]P. R. T. Schipper, O. V. Gritsenko, S. J. A. van Gisbergen, and E. J. Baerends, J. Chem. Phys. **112**, 1344 (2000).
[114]F. Wang and T. Ziegler, J. Chem. Phys. **121**, 12191 (2004).
[115]F. Wang and T. Ziegler, J. Chem. Phys. **122**, 074109 (2005).
[116]S. Hirata and M. Head-Gordon, Chem. Phys. Lett. **314**, 291 (1999).
[117]See supplementary material at http://dx.doi.org/10.1063/1.4922111 for TD-DFT and LF-DFT results on PW91 optimized geometries (Tables S1–S22), and for all non-empirically determined parameters obtained by LF-DFT procedure (Tables S23–S33).
[118]A. Klamt and G. Schuurmann, J. Chem. Soc., Perkin Trans. 2 **1993**, 799.
[119]A. Klamt, J. Phys. Chem. **99**, 2224 (1995).
[120]A. Klamt and V. Jonas, J. Chem. Phys. **105**, 9972 (1996).
[121]C. C. Pye and T. Ziegler, Theor. Chem. Acc. **101**, 396 (1999).
[122]I. B. Bersuker, *The Jahn-Teller Effect* (Cambridge University Press, 2006).
[123]M. Papai, G. Vanko, C. de Graaf, and T. Rozgonyi, J. Chem. Theory Comput. **9**, 509 (2013).
[124]J. S. Griffith, *The Theory of Transition-Metal Ions* (Cambridge University Press, Cambridge, 1964).